Surface Science 602 (2008) 1810–1818

Contents lists available at ScienceDirect

Surface Science

journal homepage: www.elsevier.com/locate/susc

freepaper.me FREE paper

Nanodroplet impact and sliding on structured polymer surfaces

Janne T. Hirvi, Tapani A. Pakkanen *

Department of Chemistry, University of Joensuu, P.O. Box 111, FIN-80101 Joensuu, Finland

ARTICLE INFO

Article history:
Received 9 January 2008
Accepted for publication 18 March 2008
Available online 23 March 2008

Keywords:
Molecular dynamics
Friction
Surface roughness
Wetting
Water
Biopolymers
Solid–liquid interfaces

ABSTRACT

A comprehensive understanding of the wetting dynamics of rough hydrophobic surfaces is necessary for the optimization of practical applications. Molecular dynamics simulations have been used to study the impact and sliding of a nanosized water droplet on nanostructured polyethylene (PE) and poly(vinyl chloride) (PVC) polymer surfaces. The impact velocity on collision with pillar surfaces mainly influences the maximal deformation of the drop from spherical and its intrusion depth between the pillars. There is no effect on the observed equilibrium state, with the exception of the most hydrophobic PE surface, but the equilibrium shape of a droplet at the Wenzel state may be asymmetrical. A bounce of the water droplet from the most hydrophobic PE surface with smaller pillars is observed at intermediate velocity. A bounce occurs at a lower impact velocity if the collision angle is decreased or the mass of the droplet is increased. The friction against sliding was higher on the PVC surfaces than on the PE surfaces due to the less hydrophobic nature of the corresponding polymer and clear pinning of the receding contact line. The sliding distances on the PVC pillar and grooved surfaces were all short and within a small range, whereas on the surfaces the differences were more substantial. The highest friction was observed on the grooved surface for sliding orthogonal to the grooves and the lowest friction was observed on the pillar surface with the smallest pillars. The friction increased with the size of the pillars due to the decreased hydrophobicity and increased resisting force of the pillar edges. The collisions with the pillar edges decreased the sliding distance on the more hydrophobic pillar surface such that it was equal to that on the grooved surface in the groove direction.

© 2008 Elsevier B.V. All rights reserved.

1. Introduction

The equilibrium water contact angle is commonly used to characterize the hydrophobicity of surfaces. The surface covered by hexagonal closest packed $-CF_3$ groups has the maximum contact angle of about 120° for smooth surfaces [1]. Higher contact angles can be achieved only on rough surfaces, like on Taro plant leaves in Fig. 1. The theoretical predictions of Wenzel [2] and Cassie and Baxter [3] describe the effect of surface roughness on hydrophobicity for different equilibrium states. Homogeneous wetting with a continuous liquid–surface interface (Fig. 2a) can be expressed mathematically by the Wenzel equation

$$\cos\theta_r^W = r\cos\theta_e, \tag{1}$$

in which θ_r^W is the Wenzel contact angle on the rough surface, θ_e is the equilibrium contact angle on the smooth surface, and r is the roughness factor defined as a ratio of the actual surface area to the projected surface area. In the Cassie state (Fig. 2b), the liquid–surface interface is heterogeneous, with air trapped between the surface structures beneath the droplet base, and the apparent contact angle (θ_r^C) is given by the equation

$$\cos\theta_r^C = \phi_s\cos\theta_e - (1-\phi_s), \tag{2}$$

in which ϕ_s is the surface fraction. The equilibrium state with the lower contact angle on the rough surface corresponds to the minimum energy state [4]. The Wenzel and Cassie equations are generally accepted, although there has recently been discussion on their validity [5–8]. They are formally based on the liquid–solid interface area beneath the droplet base, while the contact angle is dependent on the nature of the three-phase contact line.

The contact angle of a gently positioned water droplet on a rough surface provides only partial information about the wetting properties of the surface. The experimentally observed Cassie state, which is favored in many practical applications, may be metastable and separated from the global energy minimum by an energy barrier [4,9]. It has been suggested that a such Cassie state would be the key to superhydrophobicity on Lotus and Taro leaves [10]. However, the transition from the metastable Cassie state to the Wenzel state may occur due to an impact [11], an increased droplet mass [9,12], pressure [13], or mechanical vibrations [7]. The study of droplet impact dynamics, with its rich variety of possible phenomena, such as spreading, splashing, and rebound, gives

* Corresponding author. Tel.: +358 13 2513345; fax: +358 13 2513344.
E-mail address: tapani.pakkanen@joensuu.fi (T.A. Pakkanen).

0039-6028/$ - see front matter © 2008 Elsevier B.V. All rights reserved.
doi:10.1016/j.susc.2008.03.020

Fig. 1. A water droplet on a hydrophobic Taro plant leaf.

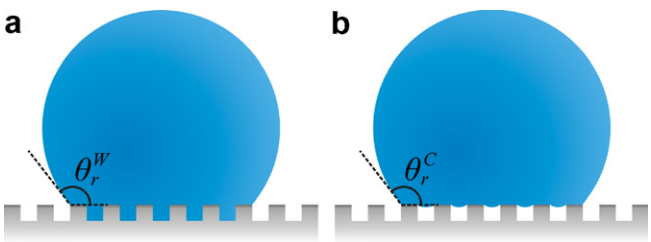

Fig. 2. Schematic views for (a) wetted and (b) composite states.

practical insight into surface wettability [14]. The maximum spread of a droplet upon impact is pronounced for a liquid with low viscosity and low surface tension and it increases with an increasing velocity and a decreasing contact angle [15,16]. A large maximum spread increases energy available for recoil and subsequent bounce from a hydrophobic surface. On a highly hydrophobic surface, an almost spherical droplet can be observed to bounce at moderate impact velocities [17]. At low velocities, a droplet attaches to the surface and at high velocities a droplet may break up and bounce partially. On a less hydrophobic surface, the extreme spread of a droplet causes splash, which occurs at lower impact velocities on a rough surface than on a smooth surface [16]. The splash can exist only in the presence of a surrounding gas phase [18]. The impact velocity and position also affect the observed equilibrium shape on chemically heterogeneous surface [19].

An experimentally measured high water contact angle, which can vary between the receding and advancing contact angles depending on how the droplet is formed, is not a guarantee that the surface has excellent water-shedding properties. The force required to move a droplet is directly proportional to contact angle hysteresis [20], which is defined as the difference between the receding and advancing contact angles. Generally, a droplet has a lower contact angle hysteresis in the Cassie state than in the Wenzel state [21–23] and hence a lower sliding angle [12]. A water droplet also slides more easily on an only slightly hydrophobic surface with a flexible, liquid-like covalently attached monolayer than on some more hydrophobic rough surfaces [24]. Even molecular level topography can affect contact angle hysteresis [25], but it can be minimized with proper design of the three-phase contact line [24,26–28]. The contact line on hydrophobic pillar surfaces in the Cassie state is more tortuous and unstable if the rectangular pillars are beveled. An increase in the ground-state energy decreases the activation energy barrier between the metastable states. Such an increase in ground-state energy causes pinning of the receding perimeter to decrease, and the receding contact angle to increase, which results in an overall decrease of the contact angle hysteresis. An increase in the pillar spacing [27] or two length scales of topography, as on hydrophobic plant leaves, increases the receding contact angle due to a decrease in the contact length [29,30]. A surface with a high apparent Cassie contact angle has a low sliding angle, which is even smaller for a larger droplet [12,31,32]. However, if the sliding angles on a pillar surface and on a grooved surface parallel and perpendicular directions are compared, it can be seen that a continuous contact line in the sliding direction and a short line in the perpendicular direction are preferred [12,33].

The preceding summary reveals the variety of complicated phenomena which affect droplet dynamics, especially on rough hydrophobic surfaces. Experimental studies and theoretical predictions have been responsible for most of our advances in understanding at the macroscopic scale, but molecular dynamics simulations offer a method for the study of these phenomena at the atomic level in nanoscale. Roughness in simulation scale limits largely to features, which are about 10 times smaller than the smallest nanostructures of the dual-scale roughness of the superhydrophobic plant leaves, while the larger micrometer roughness scale is clearly unattainable. Regardless of the differences in roughness scale and also in droplet size, simulated water contact angles on smooth [34] and structured surfaces [35,36] are in good agreement with experiments and macroscopic theories with some special characteristics. Hence, we extend our previous simulations on structured polymer surfaces [35,36] to non-zero initial velocities. A low impact velocity has only a minor influence on the shape of a simulated nanodroplet during collision with a smooth surface [37]; hence, here we also present results on the effect of high impact velocities. Actually, small droplets in simulation scale require higher velocities for the occurrence of experimentally observed phenomena. The surface effects dominates in nanoscale and an increase in the surface area due to the compression is energetically more unfavorable and additional energy is also needed to defeat the emphasized liquid-surface interactions. The variety of impact velocities, collision angles, and droplet sizes is expected to reveal the wetting dynamic differences of polyethylene (PE) and poly(vinyl chloride) (PVC) pillar surfaces with different surface fractions. A droplet actually bounces from the most hydrophobic pillar surface at intermediate velocity. Moreover, friction and its direction dependence for different surface structures was studied by comparing the sliding distances on pillar surfaces and on grooved surfaces in both the parallel and perpendicular directions.

2. Models and methods

Molecular dynamics simulations were used to study the wetting of structured PE and PVC polymer surfaces during nanodroplet impact and sliding or, to be exact, motion parallel to the surface. The initial velocities of droplets (v) varied from 10 m/s to 500 m/s. The impact on pillar surfaces was studied with collision angles ($\angle$) of 45° and 90°, of which the latter is equivalent to perpendicular collision with the surface. Sliding, which corresponds to a collision angle of 0°, was studied on both pillar and grooved PE and PVC surfaces.

The periodically structured surfaces were cut from the smooth crystalline (1 0 0) surfaces, which were duplicated from the experimental orthorhombic unit cells of PE [38] and PVC [39] crystal structures. The lateral dimensions of the surfaces were at least 160 Å and the height was eight polymer layers, of which the lowest two were complete and six layers above were partial. The grooves of $2C6P_{22}$ surfaces were cut in the direction of the polymer chains and only whole chains were removed, leaving the crystal structure otherwise undisturbed. The first part of the name $2C6P_{22}$ refers to

freepaper.me FREE paper

the complete (2C) and partial (6P) polymer layers and the two subscripted values refer to the number of remaining and removed polymer chains respectively in the period of the topmost layer. Part of the polymer chains were broken in the construction of pillar structures and the broken chains were terminated by C–H bonds in the direction of the original C–C bond. The pillar surfaces with the smallest lateral pillar dimensions, namely S6 for PE and M6 for PVC, are cut directly from the grooved surface of the corresponding polymer. The other pillar structure for both polymers has both lateral dimensions larger than the preceding surface. The names S6, M6, and L6 refer to small, medium, and large lateral pillar sizes with a height of six partial polymer layers. The surfaces with small pillars (S6) and with large pillars (L6) are the most hydrophobic of the structured PE and PVC surfaces, respectively. The most hydrophilic surfaces for both polymers are the grooved $2C6P_{22}$ surfaces [35,36]. The projected dimensional parameters, heights, and solid surface fractions (ϕ_s) of the surface structures are presented in Table 1 and visualized in Fig. 3.

A water nanodroplet consisted of simple point charge (SPC) [40] molecules for which bond distances and bond angles were fixed with the SETTLE algorithm [41]. The impact and sliding simulations on the pillar surfaces were performed for a droplet consisting of 8788 water molecules, analogous to the simulations with no initial velocity [35]. The effect of a larger momentum at impact, due to a heavier droplet, was also studied with one simulation for an eight fold larger droplet. The droplet was composed of 70,304 molecules and the radius of the free droplet was almost 8 nm. The sliding simulations on the grooved surfaces were performed for droplets consisting of 8788 and 13,500 molecules, allowing comparison with the sliding simulations on pillar surfaces and with the simulations on the grooved surfaces with no initial velocity [36].

A 300 K relaxed nanodroplet with an initial velocity was centered at a specific height on top of a frozen structured surface. For the collision simulations, the center of mass of the droplet was positioned 10 nm above the surface and for the sliding simulations, the lowest atom of a droplet was at surface level between the surface structures. In the latter case, contact between a droplet and a surface was already established at the initial configuration. The lateral dimensions of the surface were equal to those of the simulation box and the system was treated periodically. The height of the simulation box was three times as large as the maximal lateral dimension, to avoid interactions of the periodic images in the direction perpendicular to the surface plane. The equations of motion were solved in the constant volume and energy (NVE) ensemble, without an effect of temperature coupling to the velocities, using the GROMACS 3.3.1 molecular dynamics package [42]. The total simulation time with an integration time step of 2.0 fs varied from 1.0 ns to over 5.0 ns when the simulations were continued at least 0.5 ns after the stabilization of system. The analysis of the equilibration is based on the droplet velocity, and the stabilization of the height of the center of mass of the droplet and the water–surface interaction energy according to Fig. 4.

The potential energy of the system consists of intermolecular interactions among rigid water molecules and between water molecules and the frozen surface. The partial charges and Lennard–Jones 12–6 potential (3) parameters for the system are presented

Table 1
Dimensional parameters for the pillar (S6, M6, L6) and grooved ($2C6P_{22}$) structures on PE and PVC surfaces[a]

	a_x (Å)	a_y (Å)	b_x (Å)	b_y (Å)	H (Å)	ϕ_s
PE						
S6	6.7	10.0	13.6	9.7	22.2	0.167
M6	11.8	12.5	8.5	7.3	22.2	0.367
$2C6P_{22}$	∞	10.0	0.0	9.7	22.2	0.507
PVC						
M6	11.9	12.0	8.5	8.9	30.7	0.335
L6	14.4	17.3	5.9	3.7	30.7	0.584
$2C6P_{22}$	∞	12.0	0.0	8.9	30.7	0.573

[a] See Fig. 3 for explanations of parameters.

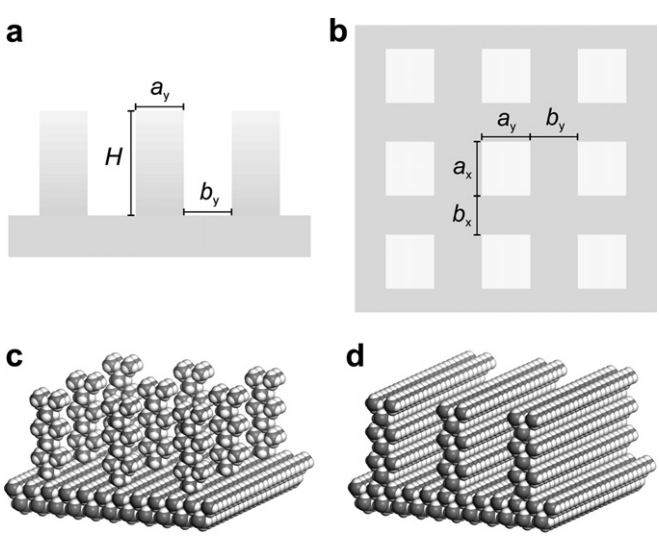

Fig. 3. Schematic views of the structure parameters from (a) the side and (b) the top and snapshots of (c) the S6 pillar structure and (d) $2C6P_{22}$ groove structure of the PE surface.

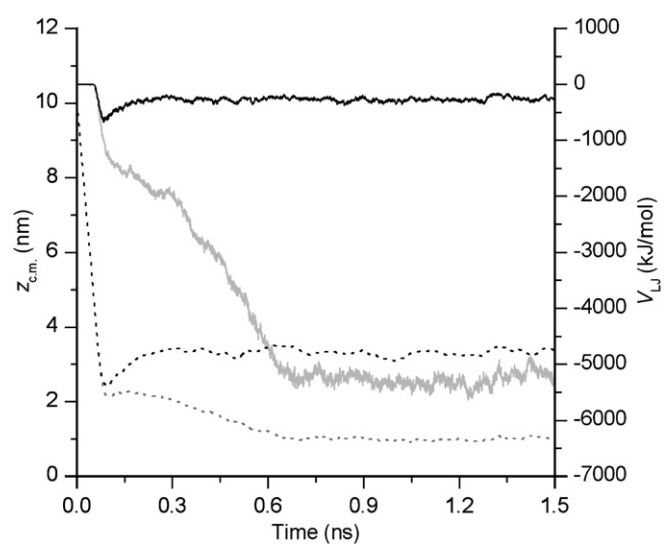

Fig. 4. The height of the center of mass of the water droplet ($z_{c.m}$) (dotted lines) and the Lennard–Jones energy of water–surface interactions (V_{LJ}) (solid lines) for the collision of a nanodroplet with the M6 PE (black) and PVC (gray) pillar surfaces with an impact velocity of 100 m/s. Different equilibrium states reflect to the equilibration times.

Table 2
Partial charges for the system

	Water	PE		PVC		
		CH_2	CH_3	CHCl	CH_2	CH_3
q_O (e)	−0.820	–	–	–	–	–
q_H (e)	0.410	0.053	0.053	0.1486	0.0990	0.0628
q_C (e)	–	−0.106	−0.159	0.0313	−0.1792	−0.1790
q_{Cl} (e)	–	–	–	−0.1987	–	–

freepaper.me FREE paper

دانلود کننده مقالات علمی freepaper.me FREE paper

Table 3
Lennard–Jones 12–6 interaction parameters for the system

	Water–water	PE–water		PVC–water		
	O/O	C/O	H/O	C/O	H/O	Cl/O
R_{ij} (Å)	3.5532322	3.7378448	3.2303345	3.6745935	3.3269082	3.6992652
ε_{ij} (kJ mol^{-1})	0.6501940	0.3832783	0.2332557	0.5487710	0.2194340	0.9472021

in Tables 2 and 3. The Lennard–Jones parameters for water–surface interactions are the geometric means of the corresponding collision diameters (σ) and well depths (ε). The interaction parameters of the polymer consistent force field (PCFF) from the Cerius[2] program were used for PE [43]. The analogous parameters for PVC were taken from the more specific force field derived especially for PVC [44,45]. A switch function from 10 Å to 11 Å was used to truncate van der Waals interactions when the neighbor searching was performed within a distance of 12 Å at every time step. A direct space cutoff for Coulombic interactions, modeled by the Particle Mesh Ewald (PME) [46,47] method with slab correction (3dc) [48], was also 12 Å and a tolerance $\varepsilon_{\mathrm{dir}} = 10^{-8}$. In the reciprocal space, a maximum grid spacing of 1.0 Å with sixth order interpolation was used.

$$V_{\mathrm{LJ}}(r_{ij}) = \varepsilon_{ij}\left(\left(\frac{R_{ij}}{r_{ij}}\right)^{12} - 2\left(\frac{R_{ij}}{r_{ij}}\right)^{6}\right) \quad (3)$$

The equilibrium shape of a nanodroplet after impact or sliding was specified with a contact angle (θ_r), which was calculated using a three-step procedure [49,50]. At first, a water density profile was defined from the coordinate data stored at intervals of 0.5 ps. On pillar surfaces, a droplet has a spherical shape, and cylindrical averaging around the center of mass of the droplet was used. However, on the grooved surfaces, a droplet shape may be asymmetrical and hence two profiles, one in the groove direction and one in the perpendicular direction, were calculated, averaging only in the line passing through the center of mass of the droplet. Next, the spherical liquid–vapor interface was defined for the density profile as the location where the density falls below 0.5 g/cm^3. Only data beyond than 8 Å from the surface was taken into account. Finally, the contact angle was determined at the intersection of the liquid–vapor interface and the surface plane.

3. Results and discussion

The impact or initial sliding velocity, varying from 10 m/s to 500 m/s, induced additional translational energy beyond the thermal kinetic energy, which was released at collision or during frictional deceleration. A quick and complete release of translational energy to other energy components took place at collision if the droplet attached to the surface in place. During lateral motion, either due to an initial collision angle of 0° or possibly after impact with a collision angle of 45°, the energy exchange was also complete but occurred slowly, together with a decrease in droplet velocity. Only partial energy exchange was observed when a droplet bounced from the surface with a velocity less than the impact velocity. Because of the frozen surfaces employed the translational energy released turned into the potential and kinetic energy of the liquid droplet and formed water gas phase.

An impact velocity of 10 m/s has hardly any effect on the temperature of a droplet and even an impact velocity or initial sliding velocity of 100 m/s increases the droplet temperature by less than 2 K. Actually, the equilibrium configuration in the Wenzel state warms up the droplet, due to the stabilization of the potential energy, approximately as much as the released translational energy corresponding to a velocity of 100 m/s. Only for the simulations with the highest initial velocity (500 m/s) could the warming, of about 25 K, be considered significant. However, a somewhat higher temperature seems to have no clear effect on the simulated contact angles and equilibrium states nor on overall behavior of the droplet on structured surfaces, but it influences evaporation of water molecules during simulation. Water vapor pressures and densities calculated with the ideal gas equation from the number of evaporated water molecules at the end of the simulation correlate with experimental values at the corresponding temperature. Simulated vapor pressures at 300–305 K vary from 0.02 to 0.08 bar and at 324–328 K from 0.17 to 0.26 bar, whereas the corresponding experimental values at 302.5 K and 326 K are 0.04 bar and 0.14 bar, respectively [51]. A heavy collision with an impact velocity of 500 m/s may slightly increase evaporation and hence also increase the simulated vapor pressures.

3.1. Impact on polyethylene pillar surfaces

The PE surface with smaller pillars (S6) is more hydrophobic than the surface with larger pillars (M6) and a gently positioned water droplet has about a 10° larger contact angle on the S6 surface than on the M6 surface [35]. The wettability difference of the PE surfaces with two pillar sizes is emphasized in the collision simulations. The simulated contact angles (θ_r) and the observed equilibrium states for a nanodroplet consisting of 8788 water molecules, after impact on PE surfaces with pillar structures, are presented in Table 4. A droplet attaches to the less hydrophobic M6 surface regardless of the impact velocity and collision angle, but may bounce from the more hydrophobic S6 surface.

The impact velocity and collision angle have no influence on the equilibrium contact angle, equilibrium state and shape of the water droplet after collision with the PE surface with larger pillars (M6). A droplet finally stabilizes at the Cassie state, touching only the tops of the pillars, with a contact angle equal to the simulated angle with no impact velocity. However, impact velocity has a drastic effect on the shape of the droplet during collision. A higher velocity causes larger deformations and the droplet shape becomes more flattened, and it intrudes deeper between the pillars, as can be seen in Fig. 5. A droplet with a velocity of 500 m/s even touches the bottom between the pillars, but finally it rises from the Wenzel state to the Cassie state. A simulated nanodroplet, even at high velocities, remains in one piece, except for evaporated water molecules, due to strong cohesive forces, and no break up or splashing

Table 4
Simulated equilibrium contact angles (θ_r) on the PE pillar surfaces for a droplet with an impact velocity (v) and a collision angle ($\angle$) with a comparison to the results for no initial velocity

v (ms^{-1})	$\angle$ (deg)	θ_r (deg)[c]	θ_r (deg)[c]
		PE S6	PE M6
0[a]	–	156.4[C]	145.8[C]
10	90	158.3[C]	143.5[C]
100	90	158.3[C]	142.7[C]
100[b]	90	180.0	–
100	45	180.0	143.8[C]
200	90	180.0	141.1[C]
500	90	161.3[C]	145.3[C]

[a] Ref. [35].
[b] A droplet consisting of 70304 water molecules.
[c] C refers to the observed composite contact.

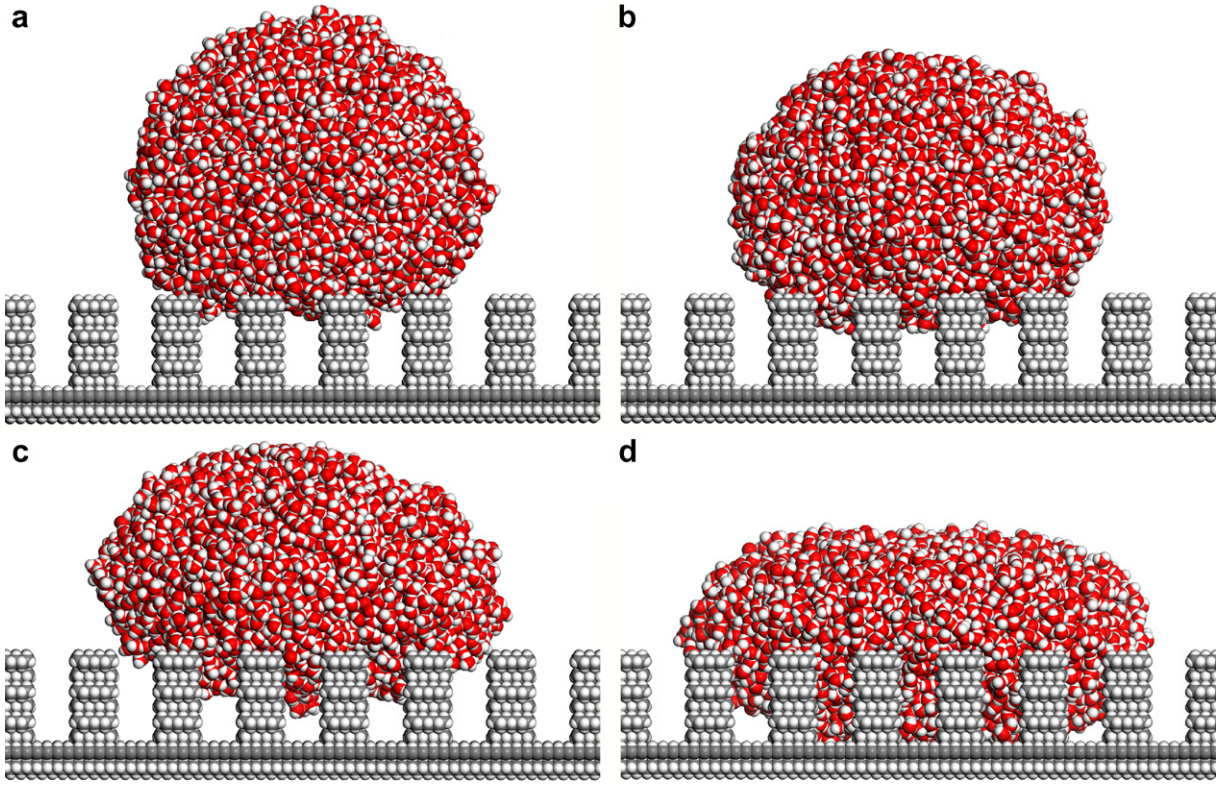

Fig. 5. The collision of a droplet with the PE pillar surface (M6) with an impact velocity of (a) 10 m/s, (b) 100 m/s, (c) 200 m/s, and (d) 500 m/s.

freepaper.me FREE paper

is observed. On the other hand, a velocity of 10 m/s has no effect on the droplet's shape at collision and the simulation is basically equal to the simulations with no impact velocity. This similarity is due to the favorable interactions between the droplet and the surface, which significantly accelerate a droplet, without or with a slow impact velocity, within the interaction distance.

On the PE surface with smaller pillars (S6), a water droplet with an impact velocity of 10 m/s or 100 m/s also equilibrates to the Cassie state with a contact angle equal to that without an impact velocity on the corresponding surface. However, a droplet with a velocity of 100 m/s almost detaches from the surface just after the impact and before stabilization on the tops of the pillars. A bounce from the surface is observed if the size of the droplet colliding with the surface is increased from 8788 to 70,304 molecules. The heavier droplet has larger momentum, which makes detachment from the surface easier. Increasing the velocity to 200 m/s also causes the droplet to bounce from the surface, according to the snapshots presented in Fig. 6. A droplet intrudes deeper between the smaller pillars of the S6 surface than the larger pillars of the M6 surface, which induces a larger repulsive force, providing the droplet with a high enough velocity to escape from the interaction field of the surface. However, if the impact velocity is increased to 500 m/s, no bounce is observed and the droplet again attaches to the S6 surface. The high impact velocity provides the droplet with enough kinetic energy to intrude all the way down to the bulk surface, which maximizes favorable water–surface interactions. The larger free space between the pillars of the S6 surface than the M6 surface also stabilize water–water interactions in the Wenzel state just after the collision and a metastable Wenzel state is actually observed. The Cassie state is achieved stepwise and slowly in about 5 ns.

A nanodroplet consisting of 8788 water molecules has not quite enough kinetic energy to be able to detach from the S6 surface after a collision with an impact velocity of 100 m/s. A bounce is observed if the size of the droplet is increased or the impact velocity is doubled to 200 m/s. Detachment can also be made easier by decreasing the collision angle, in which case not all of the translational energy is directed perpendicular to the surface. The decrease of the collision angle from 90° to 45° enables a droplet to bounce from the S6 surface after a collision with an impact velocity of 100 m/s. On the less hydrophobic M6 surface, a droplet with an equal impact velocity attaches to the surface even though the collision angle is decreased from 90° to 45°, but now the translational energy enables the droplet to continue motion 13.6 nm on top of the pillars before it stops.

3.2. Impact on poly(vinyl chloride) pillar surfaces

In contrast to the PE surfaces with pillars, the PVC surface with larger pillars (L6) is more hydrophobic than the surface with smaller pillars (M6). A gently positioned water droplet on larger pillars stabilizes to the Cassie state with a contact angle about 10° larger than on the M6 surface in the Wenzel state [35]. The simulated equilibrium contact angles (θ_r), with the corresponding equilibrium states, for a nanodroplet consisting of 8788 water molecules after collision with the PVC pillar surfaces are presented in Table 5. The equilibrium contact angles and states after collision are equal to those obtained without an impact with only one exception and no drastic differences between the two pillars sizes are observed, in contrast to the more hydrophobic PE surfaces.

The impact velocity mainly has an effect on the shape of the droplet on collision with the PVC pillar surfaces, and even then only at high velocities. A spherical droplet shape is preserved on collision with an impact velocity of 10 m/s. No drastic change in droplet shape is observed if impact velocity is increased to 100 m/s, but the translational energy enables a direct but partial intrusion between the pillars of the M6 surface. The intrusion between the larger pillars of the L6 surface is only minor, even if the impact velocity is increased to 500 m/s, whereas the bulk

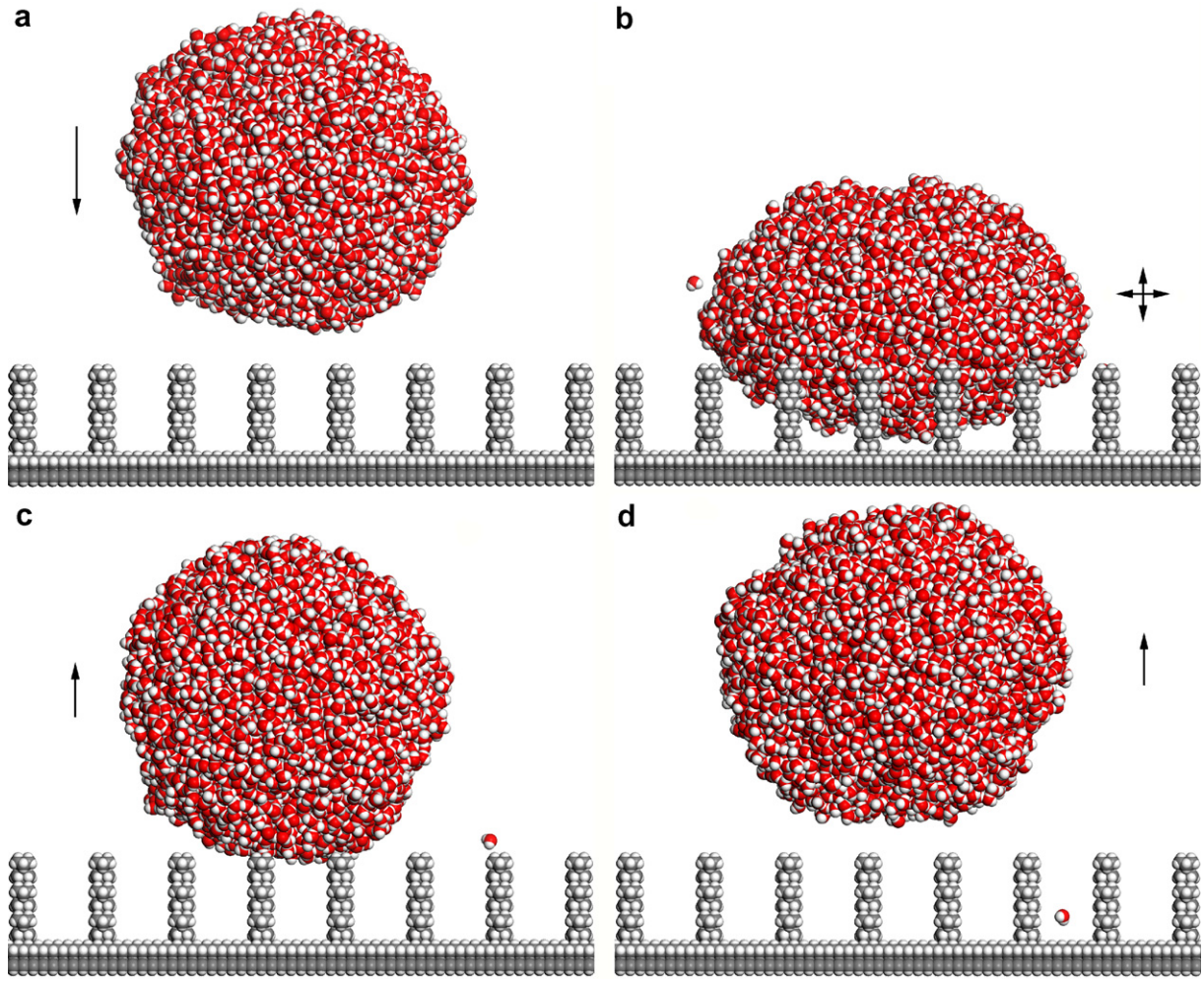

Fig. 6. Snapshots at times (a) 25 ps, (b) 53.5 ps, (c) 150 ps, and (d) 200 ps of the collision of a nanodroplet with the PE pillar surface (S6) with an impact velocity of 200 m/s. The arrows indicate the direction and magnitude of droplet velocity.

Table 5
Simulated equilibrium contact angles (θ_r) on the PVC pillar surfaces for a droplet with an impact velocity (v) and a collision angle ($\angle$) with a comparison to the results for no initial velocity

v (ms^{-1})	$\angle$ (deg)	θ_r (deg)[b]	θ_r (deg)[b]
		PVC M6	PVC L6
0[a]	–	106.2[W]	116.9[C]
10	90	105.8[W]	116.9[C]
100	90	106.5[W]	117.2[C]
100	45	106.3[W]	116.7[C]
500	90	91.2/103.1[Wc]	114.5[C]

[a] Ref. [35].
[b] W refers to the observed wetted contact and C to the observed composite contact.
[c] The values correspond to the projected contact angles in the x and y directions.

surface between the pillars of the M6 surface is reached directly on collision at high impact velocity. A nanodroplet flattens out totally on impact with a velocity of 500 m/s, regardless of the surface, but the spherical shape of the cap of the droplet is rapidly restored. Decrease in the collision angle from 90° to 45° results in receding perimeter of a droplet being stuck in place, while the advancing perimeter still continues moving; however, the droplet attaches almost in place and no clear lateral motion is observed.

The Wenzel state after a low energy collision on the PVC surface with smaller pillars (M6) is achieved slowly by the slow intrusion of water molecules between the pillars. An increase in impact velocity enables at least partial direct intrusion and speeds up the transition. Extremely high velocities may lead directly to achievement of the complete Wenzel state at collision and even induce asymmetrical equilibrium shapes. On the M6 surface, the nanodroplet equilibrium contact angle in the direction of the slightly smaller pillar gap is over 10° smaller than in the perpendicular direction after collision with a velocity of 500 m/s.

3.3. Sliding on pillar surfaces

A decrease of the collision angle to 0° corresponds to a nanodroplet sliding on a surface with an initial velocity. Actually, first touches to the surface give rise to the rotational energy of the droplet, but no clear rolling is observed and the rotational energy fades away while the lateral motion still continues by sliding. The sliding or more precisely lateral motion distance of a nanodroplet in the direction of the initial velocity was used as a measure of surface friction. The momentary rotational energy and the shape of the moving droplet provide additional valuable information about the nanodroplet dynamics on pillar and grooved surfaces.The sliding distances (d) and the simulated contact angles (θ_r), with the observed equilibrium states for a nanodroplet consisting of 8788 water molecules, on the PE and PVC surfaces with pillars are given in Table 6. The sliding distances are longer on the more hydrophobic PE surfaces than on the PVC surfaces, indicating lower friction

freepaper.me FREE paper

Table 6
The sliding distance (d) in x direction on the pillar surfaces for a droplet of 8788 molecules with non-zero initial velocity (v) and the simulated equilibrium contact angles (θ_r) with a comparison to the results for no initial velocity

v (ms^{-1})	d (nm)	θ_r (deg)[b]	d (nm)	θ_r (deg)[b]
	PE S6		PE M6	
0[a]	0	156.4[C]	0	145.8[C]
100	95.9	154.1[C]	24.1	143.5[C]
500	∞	180.0	274.0	145.9[C]
	PVC M6		PVC L6	
0[a]	0	106.2[W]	0	116.9[C]
100	8.9	89.2/100.3[Wc]	7.8	116.9[C]
500	46.8	106.8[W]	33.3	112.6[C]

[a] Ref. [35].
[b] W refers to the observed wetted contact and C to the observed composite contact.
[c] The values correspond to the projected contact angles in the x and y directions.

due to a higher contact angle and a smaller water-surface contact area. Lower friction for the both polymers is observed if the size of the pillars is decreased, even though the equilibrium contact angle on the PVC surface with smaller pillars (M6) is lower than on the PVC surface with larger pillars (L6) due differences in the equilibrium states. However, comparison of the results for the PE and PVC M6 surfaces reveals that the motion on the PVC surface is more hindered, even if the pillars of the PVC surface are somewhat smaller than the pillars of the PE surface.

The initial sliding velocity has no effect on the equilibrium contact angle and state on the PE pillar surfaces if a droplet stays attached to the surface. The shape of a droplet is well preserved while it is in motion, with an initial velocity of 100 m/s, and the sliding distance on the larger pillars (M6) is one-fourth of that on the more hydrophobic smaller pillars (S6). If the velocity on the M6 surface is increased from 100 m/s to 500 m/s, the sliding distance increases by approximately a factor of 10. Classical mechanics predicts an increase proportional to the square of the velocity ratio, predicting a 25 times longer sliding distance if the friction coefficient remains unchanged. Actually, deformation of the spherical shape of a droplet in motion with a high velocity is observed

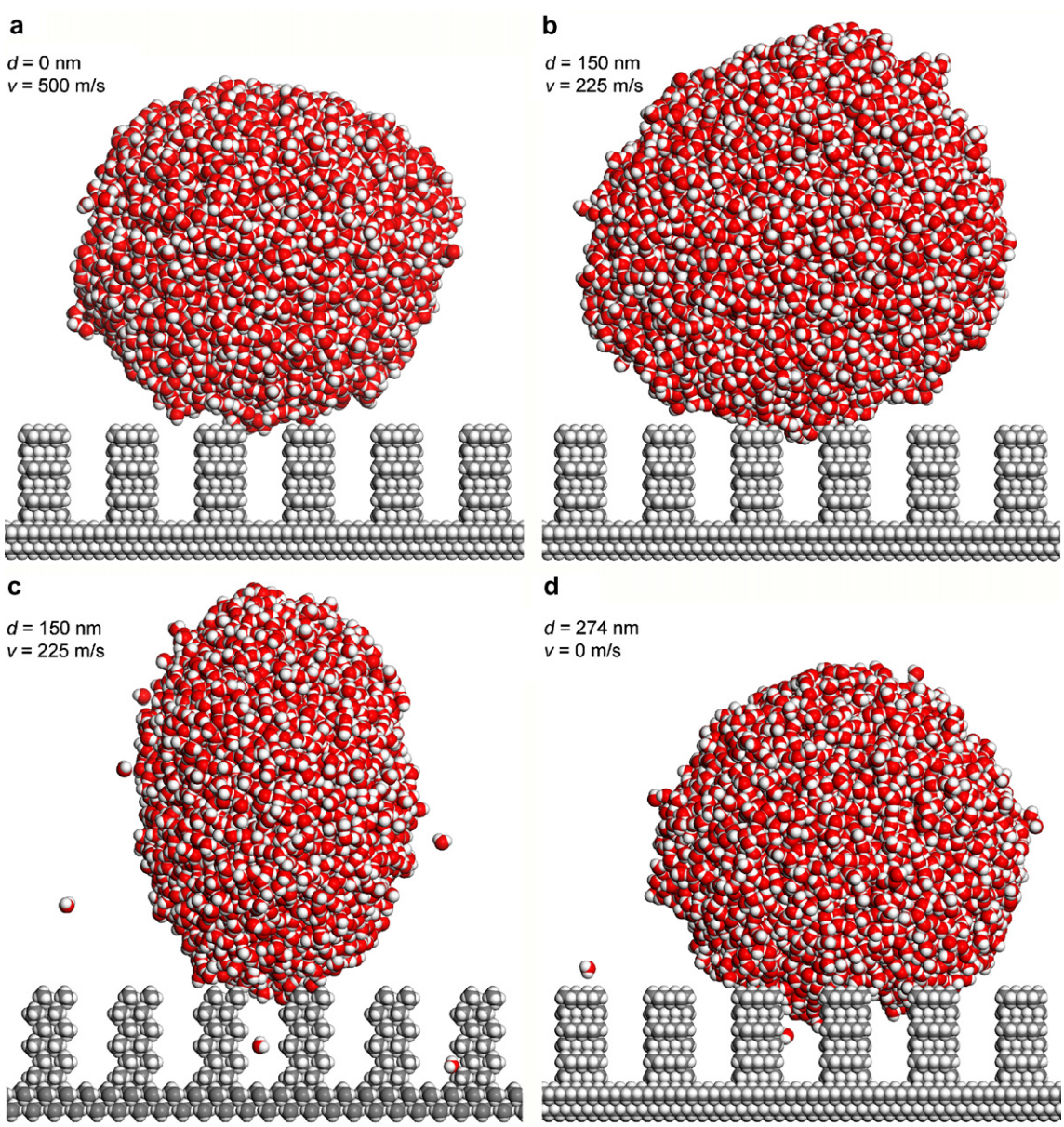

Fig. 7. Snapshots at times (a) 0 ps, (b) 480 ps (x projection), (c) 480 ps (y projection), and (d) 3000 ps showing the shape of a moving nanodroplet on the PE pillar surface (M6) with an initial velocity of 500 m/s.

freepaper.me FREE paper

due to the increased frictional forces. The projected area of a droplet increases in the direction of motion, like a rolling snowball, while the perpendicular projected area is squeezed as shown in Fig. 7. The spherical shape of the nanodroplet on the PE surface with larger pillars (M6) is re-established when the velocity decreases and the droplet stops. On the PE surface with smaller pillars (S6) deformation of a sliding droplet continues, forming a rotating rod, which detaches from the surface until finally a spherical shape returns.

On the PVC pillar surfaces, differences in the sliding distances are much smaller than on the more hydrophobic PE pillar surfaces. The sliding distance increases by less than a factor of 1.5 if the size of the pillars is decreased and by approximately a factor of 5 if the initial velocity is increased from 100 m/s to 500 m/s. The droplet shape deviates from spherical with a velocity of 100 m/s, but this effect is pronounced only at higher velocities, as can be seen from Fig. 8. The receding perimeter of the droplet sticks to the surface due to the more hydrophilic nature of the PVC surface than the corresponding PE surface. The elongation of a droplet may even lead to an asymmetric Wenzel state for which the contact angle in the direction of the motion is smaller than that in the perpendicular direction.

3.4. Sliding on grooved surfaces

The movement of nanodroplets on the grooved polymer surfaces was studied with two droplet sizes. A smaller droplet, consisting of 8788 water molecules, enabled a direct comparison with the results from the corresponding pillar surfaces, and a larger droplet, consisting of 13,500 water molecules, allowed a comparison of the simulations with no initial velocity [36]. The sliding distances (d) and the simulated contact angles parallel ($\theta_r^{\parallel}$) and perpendicular ($\theta_r^{\perp}$) to the grooves with the observed equilibrium states for both droplet sizes are presented in Table 7.

The spherical symmetry of the droplet is maintained on the grooved PE surfaces and the simulated contact angles and equilibrium states are equal to those without an initial velocity. The sliding distances are affected by the size of the droplet, being 1.2–1.4 times longer for the larger droplet than for the smaller nanodroplet. However, the ratio of the sliding distances in the groove direction and in the perpendicular direction on the PE surface is approximately 2.5 for the both droplet sizes. The movement is hindered in the direction perpendicular to the grooves, which can also be seen as a momentary increase in the rotational energy of a droplet moving in that direction due to collisions with the groove edges.

The smallest friction on the structured PE surfaces is observed for the movement of a nanodroplet on the smallest pillars (S6), with a sliding distance of 95.9 nm. If the pillars of the S6 surface are connected to the stripes of the $2C6P_{22}$ surface, the sliding distance decreases to one-fourth of that on the S6 pillar surface. This is a consequence of the increased surface fraction beneath the moving droplet, which decreases the Cassie contact angle by over 20°. However, the sliding distance on the grooved PE surface in the groove direction is equal to the sliding distance on the M6 pillar surface, although the water contact angle on the grooved surface is over 10° smaller than on the pillar surface. The resistance of the pillar edges of the M6 surface offsets the benefit from the higher hydrophobicity. A discontinuous contact line in the sliding

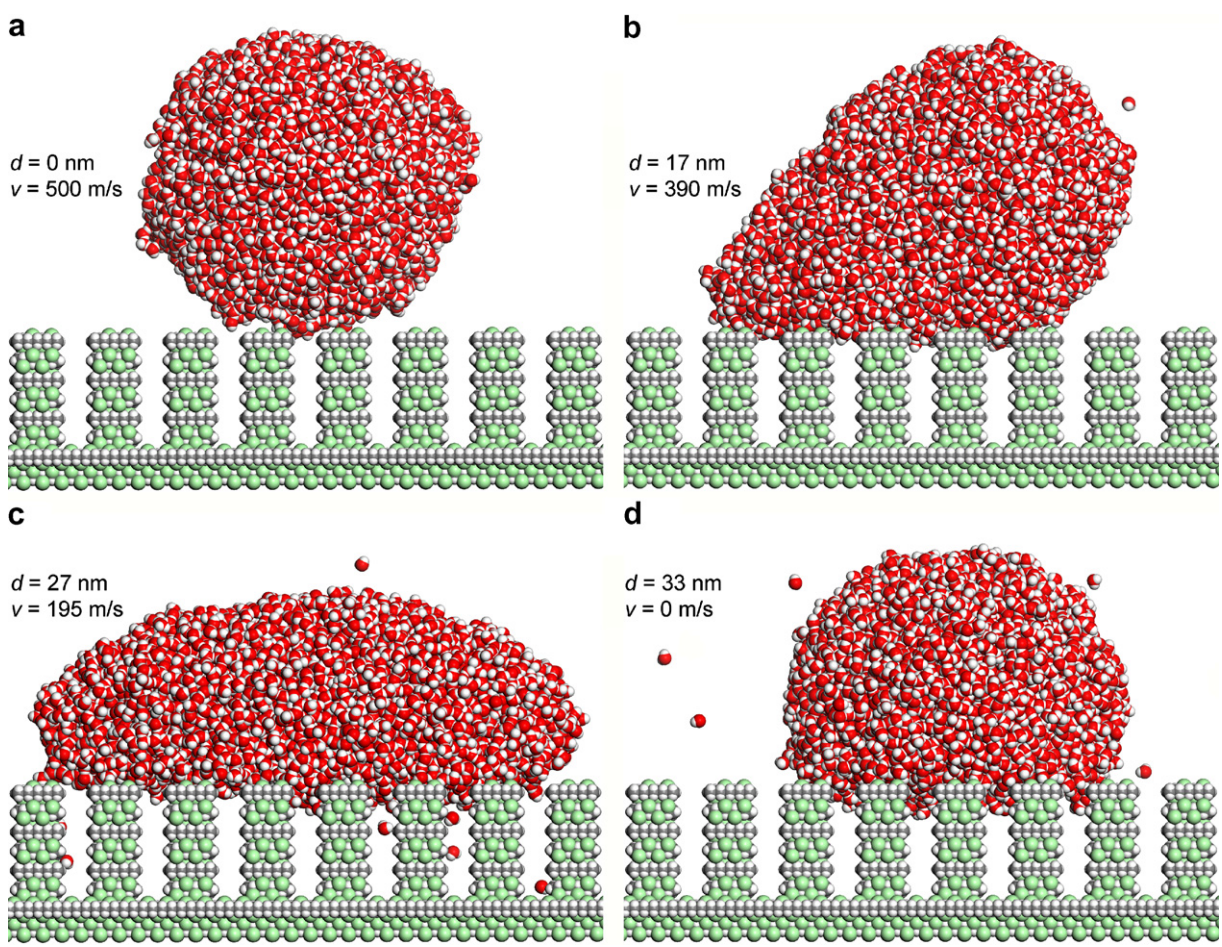

Fig. 8. Snapshots at times (a) 0 ps, (b) 37 ps, (c) 70 ps, and (d) 1000 ps showing the shape of a moving nanodroplet on the PVC pillar surface (L6) with an initial velocity of 500 m/s.

FREE paper freepaper.me دانلود کننده مقالات علمی

Table 7
The sliding distance (d) parallel or perpendicular to the grooves for a droplet with a non-zero initial velocity (v) in the corresponding direction and the projected equilibrium contact angles parallel ($\theta_r^{\parallel}$) and perpendicular ($\theta_r^{\perp}$) to the grooves with a comparison to the results for no initial velocity

v (ms^{-1})	d (nm)	$\theta_r^{\parallel}$ (deg)[b]	$\theta_r^{\perp}$ (deg)[b]
PE 2C6P$_{22}$/8788			
0	–	–	–
100$^{\parallel}$	22.4	130.6^{C}	129.7^{C}
100$^{\perp}$	9.5	134.5^{C}	130.5^{C}
PE 2C6P$_{22}$/13,500			
0[a]	0	133.9^{C}	134.9^{C}
100$^{\parallel}$	31.2	131.7^{C}	133.7^{C}
100$^{\perp}$	11.9	132.8^{C}	133.3^{C}
PVC 2C6P$_{22}$/13,500			
0[a]	0	58.4^{W}	88.0^{W}
100$^{\parallel}$	8.4	53.6^{W}	84.4^{W}
100$^{\perp}$	6.4	54.2^{W}	65.4^{W}

[a] Ref. [36].
[b] W refers to the observed wetted contact and C to the observed composite contact.

direction and a continuous one in the perpendicular direction maximize the friction and hence the highest friction is observed on the grooved surface in the direction perpendicular to the grooves. A droplet on the structured surfaces moves more freely if the water–surface contact area is low and there is a continuous contact line in the direction of the motion [12].

The sliding distances on the more hydrophilic PVC surfaces are quite short and no significant difference due to the mass of the droplet was expected, so the sliding simulations on the grooved PVC surface were performed only for the larger droplet. Comparison with the results for the PVC pillar surfaces with an initial sliding velocity of 100 m/s reveals that all the sliding distances are almost identical, varying from 6.5 to 8.9 nm. However, the highest friction is once again observed on the grooved surface when the motion is perpendicular to the grooves, and the lowest is seen on the surface with smaller pillars (M6), which is cut from the 2C6P$_{22}$ grooved surface. The droplet stretches slightly in the sliding direction, which is due to sticking of the receding perimeter of the droplet to the PVC surface. Elongation during sliding perpendicular to the grooves causes the droplet to spread to one extra groove, and hence the projected contact angle perpendicular to the grooves is smaller than the corresponding one with no initial velocity or with a velocity in the groove direction.

4. Conclusions

Dynamic wetting of structured PE and PVC polymer surfaces on collision and sliding of a nanosized water droplet were studied by molecular dynamics simulations. Collisions on the pillar surfaces were simulated with a variety of impact velocities and collision angles. An impact velocity of 10 m/s has no effect on the shape of a droplet during collision but at higher velocities, droplet flattening and intrusion between the pillars occurs and increases with an increasing velocity. The final equilibrium shape and state are mainly independent of impact velocity. However, an asymmetric droplet shape at the Wenzel state was observed on the most hydrophilic PVC surface after a high velocity collision, and a bounce of the droplet from the most hydrophobic PE surface was observed at intermediate collision velocity. If the collision angle was decreased or the mass of a droplet was increased, a bounce occurred at lower velocities.

Friction against lateral motion on the pillar and grooved surfaces was studied based on the sliding distances. The sliding distance increased with an increase in initial velocity and mass of the droplet, and with a decrease in the surface fraction. The differences in the sliding distances were more pronounced on the more hydrophobic PE surfaces than on the less hydrophobic PVC surfaces due to the smaller liquid–surface contact area and lower friction. Sliding on the grooved surfaces is favored in the direction of a continuous contact line and hence the friction in the groove direction was smaller than in the perpendicular direction. Actually, the maximal friction is observed for sliding perpendicular to the grooves because there is a continuous contact line orthogonal to the sliding direction. The corresponding contact line on the pillar surfaces is discontinuous, like the one in the sliding direction. A discontinuity in the sliding direction on the one hand increases the friction due the collisions with the pillar edges, and on the other hand decreases it due to the smaller liquid–surface contact area in comparison to sliding on the grooved surface in the groove direction. Sliding distance on the grooved surface in the groove direction is comparable to that on a more hydrophobic pillar surface.

References

[1] T. Nishino, M. Meguro, K. Nakamae, M. Matsushita, Y. Ueda, Langmuir 15 (1999) 4321.
[2] R.N. Wenzel, Ind. Eng. Chem. 28 (1936) 988.
[3] A.B.D. Cassie, S. Baxter, Trans. Faraday Soc. 40 (1944) 546.
[4] N.A. Patankar, Langmuir 19 (2003) 1249.
[5] C.W. Extrand, Langmuir 19 (2003) 3793.
[6] L. Gao, T.J. McCarthy, Langmuir 23 (2007) 3762.
[7] E. Bormashenko, R. Pogreb, G. Whyman, M. Erlich, Langmuir 23 (2007) 6501.
[8] G. McHale, Langmuir 23 (2007) 8200.
[9] N.A. Patankar, Langmuir 20 (2004) 7097.
[10] A. Marmur, Langmuir 20 (2004) 3517.
[11] B. He, N.A. Patankar, J. Lee, Langmuir 19 (2003) 4999.
[12] Z. Yoshimitsu, A. Nakajima, T. Watanabe, K. Hashimoto, Langmuir 18 (2002) 5818.
[13] J. Bico, C. Marzolin, D. Quéré, Europhys. Lett. 47 (1999) 220.
[14] A.L. Yarin, Annu. Rev. Fluid Mech. 38 (2006) 159.
[15] T. Mao, D.C.S. Kuhn, H. Tran, Aiche J. 43 (1997) 2169.
[16] Š. Šikalo, M. Marengo, C. Tropea, E.N. Ganić, Exp. Therm. Fluid Sci. 25 (2002) 503.
[17] D. Richard, D. Quéré, Europhys. Lett. 50 (2000) 769.
[18] L. Xu, W.W. Zhang, S.R. Nagel, Phys. Rev. Lett. 94 (2005) 184505.
[19] J. Léopoldès, A. Dupuis, D.G. Bucknall, J.M. Yeomans, Langmuir 19 (2003) 9818.
[20] C.G.L. Furmidge, J. Colloid Sci. 17 (1962) 309.
[21] R.E. Johnson Jr, R.H. Dettre, Adv. Chem. Ser. 43 (1964) 112.
[22] C.W. Extrand, Langmuir 18 (2002) 7991.
[23] G. McHale, N.J. Shirtcliffe, M.I. Newton, Langmuir 20 (2004) 10146.
[24] W. Chen, A.Y. Fadeev, M.C. Hsieh, D. Öner, J. Youngblood, T.J. McCarthy, Langmuir 15 (1999) 3395.
[25] A.Y. Fadeev, T.J. McCarthy, Langmuir 15 (1999) 3759.
[26] J.P. Youngblood, T.J. McCarthy, Macromolecules 32 (1999) 6800.
[27] D. Öner, T.J. McCarthy, Langmuir 16 (2000) 7777.
[28] L. Gao, T.J. McCarthy, Langmuir 22 (2006) 6234.
[29] L. Gao, T.J. McCarthy, Langmuir 22 (2006) 2966.
[30] L. Gao, T.J. McCarthy, Langmuir 22 (2006) 5998.
[31] M. Miwa, A. Nakajima, A. Fujishima, K. Hashimoto, T. Watanabe, Langmuir 16 (2000) 5754.
[32] P. Roura, J. Fort, Langmuir 18 (2002) 566.
[33] L. Feng, S. Li, Y. Li, H. Li, L. Zhang, J. Zhai, Y. Song, B. Liu, L. Jiang, D. Zhu, Adv. Mater. 14 (2002) 1857.
[34] J.T. Hirvi, T.A. Pakkanen, J. Chem. Phys. 125 (2006) 144712.
[35] J.T. Hirvi, T.A. Pakkanen, J. Phys. Chem. B 111 (2007) 3336.
[36] J.T. Hirvi, T.A. Pakkanen, Langmuir 23 (2007) 7724.
[37] F. Gentner, R. Rioboo, J.P. Baland, J. De Coninck, Langmuir 20 (2004) 4748.
[38] S. Kavesh, J.M. Schultz, J. Polym. Sci. Part A-2 8 (1970) 243.
[39] C.E. Wilkes, V.L. Folt, S. Krimm, Macromolecules 6 (1973) 235.
[40] H.J.C. Bederdsen, J.P.M. Postma, W.F. van Gunsteren, J. Hermans, in: B. Pullman (Ed.), Intermolecular Forces, vol. 14, Reidel, Dordrecht, 1981, p. 331.
[41] S. Miyamoto, P.A. Kollman, J. Comput. Chem. 13 (1992) 952.
[42] D. van der Spoel, E. Lindahl, B. Hess, G. Groenhof, A.E. Mark, H.J.C. Berendsen, J. Comput. Chem. 26 (2005) 1701.
[43] Cerius^2 version 4.8, Accelrys, Cambridge, 2002.
[44] G.D. Smith, R.L. Jaffe, D.Y. Yoon, Macromolecules 26 (1993) 298.
[45] G.D. Smith, P.J. Ludovice, R.L. Jaffe, D.Y. Yoon, J. Phys. Chem. 99 (1995) 164.
[46] T. Darden, D. York, L. Pedersen, J. Chem. Phys. 98 (1993) 10089.
[47] U. Essmann, L. Perera, M.L. Berkowitz, T. Darden, H. Lee, L.G. Pedersen, J. Chem. Phys. 103 (1995) 8577.
[48] I.-C. Yeh, M.L. Berkowitz, J. Chem. Phys. 111 (1999) 3155.
[49] M.J. de Ruijter, T.D. Blake, J. De Coninck, Langmuir 15 (1999) 7836.
[50] T. Werder, J.H. Walther, R.L. Jaffe, T. Halicioglu, P. Koumoutsakos, J. Phys. Chem. B 107 (2003) 1345.
[51] D.E. Gray (Ed.), American Institute of Physics Handbook, third ed., McGraw-Hill, New York, 1982. Reissue.

دانلود کننده مقالات علمی freepaper.me FREE paper